

The Comparison of the Accuracy of two Mathematical Models, concerning Dynamics of the Slewing Cranes

Boris Jerman

Lecturer

University of Ljubljana
Faculty of Mechanical Engineering

Nowadays the mathematical simulations of the real-world problems can be and are expected to be very accurate. The mathematical models used for such simulations must be therefore of the appropriate complexity. On the other hand the number of degrees of freedom and related number of the equations of the model must be preserved on the fairly low level, insuring the acceptable processing times which are, of course, different for different purposes of the simulations. In the paper the basic and the enhanced mathematical models of a slewing crane during slewing motion are presented and the development of the enhanced model from the basic model is described including the procedure of reduction of the degrees of freedom. The results of the simulations and of the measurements are compared and in the case of the enhanced mathematical model an obvious improvement of the agreement is estimated.

Keywords: *Non-linear Dynamical Systems, Slewing Motion, Reduction of Degrees of Freedom, Measurements.*

1. INTRODUCTION

A study of slewing cranes and possible improvements to their performance is a study with a real-life application, because these types of crane are widely used in everyday transport operations. The operation of slewing cranes involves three main motions: the slewing motion of the jib, the radial movement of the load suspension point and the hoisting of the load. In this paper, the slewing motion of a crane, during which the spatial motion of the suspended load is introduced [1], was looked at in more detail.

The majority of published papers and conference contributions on payload dynamics deal with control strategies and techniques for load-swing suppression where the mathematical models [2-8] (for the list of other models see [9] and [10]) can be simplified to a great extent.

Although the dynamic loads caused by the crane's accelerations and decelerations represent an important part of the loadings of the crane's steel structure [10], studies of the dynamics of the payload and the influence of payload-swinging on the loading (either those that consider the linear motion of the load suspension point [11-16] or those that consider the curved motion of the suspension point [17-24]) have not been investigated to the same extent.

In order to determine the dynamic loads, more complex models must be used. Recent reports suggest the use of more complex models for control purposes too [10]. For these reasons, a mathematical model of a

general-type slewing crane was developed [9], taking into account most of the frequently neglected features.

In the paper the basic and the enhanced mathematical models of a slewing crane during slewing motion are presented and the procedure of the development of the enhanced model from the basic model is described as is the procedure of reduction of degrees of freedom. The results of the basic and enhanced mathematical model are compared with the measured results and an obvious improvement of the agreement of the simulated and measured results was estimated.

2. THE MATHEMATICAL MODELS

2.1 The basic mathematical model

The basic non-linear mathematical model of the load sway during the slewing motion (Fig. 1) which has no restriction with regard to small angles of the load sway is briefly introduced. For details see [9]. The model is based on the following assumptions: the influences of the masses of the crane's structure are represented by point masses m_i and the moment of inertia J_1 ; the elements connecting the masses are weightless. Their stiffness and damping [25] are represented by the corresponding stiffness and damping coefficients k_i and d_i ; the time-velocity profile of the motor's driving shaft $\dot{\varphi}_0(t)$ is used as a system input; the friction in the slewing ring is represented by the moment of friction M_{FR} ; the air resistance is represented by the forces of the proper magnitudes and directions acting on the point masses m_2 and m_3 .

Second-order Lagrange equations were used for deriving the system of seven non-linear differential equations of motion with non-constant coefficients. The

Received: September 2006, Accepted: December 2006

Correspondence to: Dr Boris Jerman, Lecturer

University of Ljubljana, Faculty of Mechanical Engineering,
Aškerčeva 6, 1000 Ljubljana, Slovenia

E-mail: boris.jerman@fs.uni-lj.si

system was solved numerically by using the Runge-Kutta method.

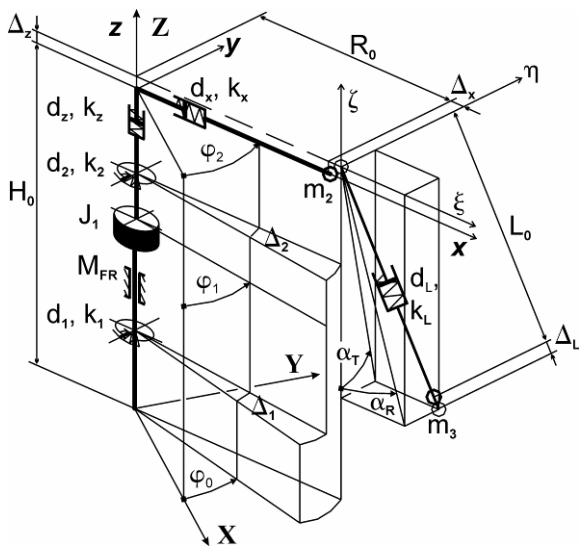


Figure 1. The basic mathematical model of a general-type slewing crane

For the numerical solution of the basic non-linear mathematical model a computer program was developed. In order to confirm the model, also a materialized model of a crane was built [9] and the measurements of seven different quantities were carried out (the radial and tangential angle (α_R and α_T in Fig. 1) of the swinging of the load were measured at MP 1 and 2 (see Fig. 2), the bending moments on the jib, around the y -axis and around the z -axis (MP 3 and 4), the torsion moment on the torsion shaft (MP 5), the angles of rotation of the driving shaft (MP 7) and of the slewing platform (MP 6)).

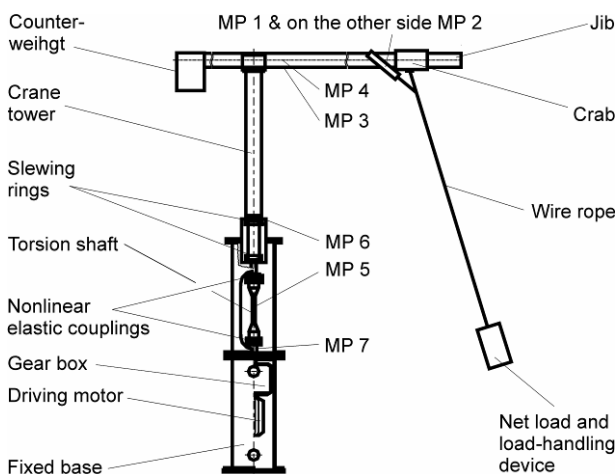


Figure 2. The materialized model of a slewing crane

The results of the simulations (with the input data from the material model) and measurements were compared. Although the agreement of the results is fairly high, especially when the qualitative agreement is considered, the quantitative differences of some of the peak values show that the model should be enhanced (see next chapter and [9]).

2.2 The enhanced mathematical model

In this sub-section the enhanced non-linear mathematical model of the load sway during the slewing motion (Fig. 3) is briefly introduced. The model was designed on the basis of the experiences with the basic mathematical model and the measurements.

The differences of the results of the individual quantities were studied carefully and the conclusion was made that the description of the tower of the crane and the description of the effects of the counter-weight must be enhanced. For this reason the moment of inertia J_4 and the point mass m_5 were added at the top of the tower (see Fig. 3).

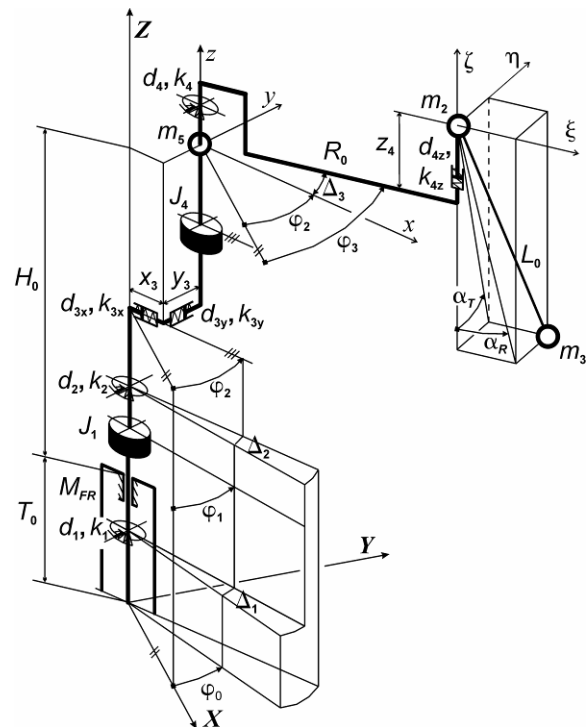


Figure 3. The enhanced mathematical model of a general-type slewing crane

By these changes, the number of the degrees of freedom of the model would increase by four and therefore the number of the equations of motion would increase respectively by four from 7 to 11. This increase in the number of equations would more than double the computing time of the numerical solution and therefore the reduction of the degrees of freedom was implemented in such a way that those with less influence were eliminated.

2.3 Determination of the influence of the individual parameters and selection of the insignificant degrees of freedom

For the estimation of the influence of the individual degrees of freedom the following procedure was implemented. The input data from the real-world tower crane was used. The corresponding parameters were selected, representing the properties of the crane's steel structure:

- the stiffness characteristics k_1 and damping characteristics d_1 are the properties of the connecting elements between the motor shaft and the rotating platform in terms of torsion (around the z -axis). Both of them are non-linear;
- the stiffness coefficient k_2 and damping coefficient d_2 are the properties of the rotating platform (or tower) and the bending stiffness of the jib, both around the z axis. These influences are combined together because both of them contribute to the shift of the mass m_2 in y direction of the local coordinate system xyz ;
- the stiffness coefficient k_x and damping coefficient d_x are the properties of the rotating platform (or tower) in terms of bending around the y axis and the stiffness of the jib in terms of the tensile deformation in x direction. These influences are combined together because both of them contribute to the shift of the mass m_2 in x direction of the local coordinate system xyz ;
- the stiffness coefficient k_z and damping coefficient d_z are the properties of the rotating platform (or tower) in terms of the tensile deformation in the z direction and the stiffness of the jib in terms of the bending around the y axis. These influences are combined together because both of them contribute to the shift of the mass m_2 in z direction of the local co-ordinate system xyz ;
- the stiffness coefficient k_L and damping coefficient d_L are the properties of the payload-carrying rope in terms of the tensile deformation along the rope length;
- the coefficient $d_{ar 2}^i$ of air resistance on mass m_2 in i -direction ($i = x, y, z$) and the coefficient $d_{ar 3}$ of air resistance on mass m_3 ;

A wide variety of simulations with different combinations of the input parameters was executed. For every combination considered, more of the simulations were calculated where the observed parameter vary from the value (close to) zero to the double the nominal value (200%) whereas the other parameters stay constant.

The following cycle was observed: constant acceleration ($\ddot{\varphi}_0 = \text{const}$) of rotation from 0 to 7 seconds, rotation with the constant rotating speed ($\dot{\varphi}_0 = \text{const}$) from 7 to 19 seconds, constant deceleration from 19 till 26 seconds and finally observation of the cranes structure after the stopping of the rotation ($\dot{\varphi}_0 = 0$) from 26 till 100 seconds.

The results are presented in 3-D graphs (Figs. 4 till 9) where the following quantities are plotted on the vertical axis against the time and against the changing value of the observed parameter: load swinging angle in the radial α_R and tangential α_T directions, the bending moment in the jib around the z -axis (M_z), the bending

moment in the jib around the y -axis (M_y) and the torsion moment in the driving shaft (M_t).

When the stiffness characteristics k_1 is varied, the following changes are observed. The values of the radial swinging angle α_R (Fig. 4) are increasing in the phase of acceleration and are decreasing in the phase of rotation with the constant speed when the stiffness k_1 is increasing. After the rotation stops the strong increase of the swinging angle is observed when the stiffness increases from 50 % to 100 % of the nominal value. Further increasing of the stiffness causes the decreasing of the swinging angle.

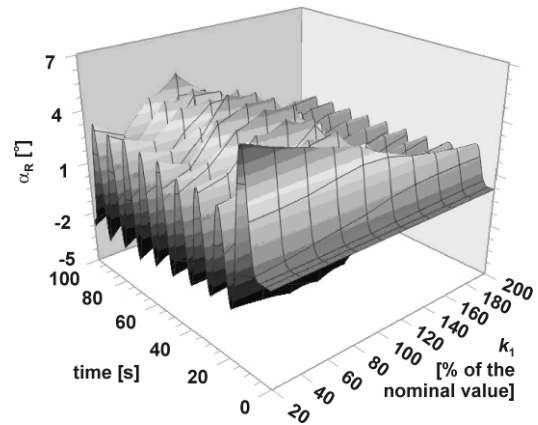


Figure 4. The load swinging angle in the radial direction α_R , when the influence of the parameter k_1 is observed

The values of the tangential swinging angle α_T (Fig. 5) are, similar to the α_R , increasing in the phase of acceleration when the stiffness k_1 is increasing.

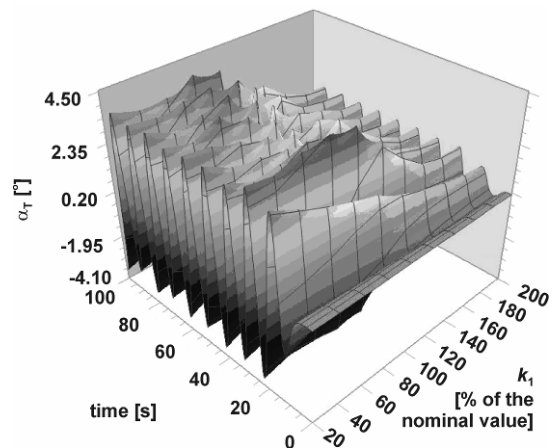


Figure 5. The load swinging angle in the tangential direction α_T , when the influence of the parameter k_1 is observed

The presented graphs clearly show the influence of the parameter k_1 . The influence is even more noticeable, when the internal moments are observed. As an example the bending moment M_z is introduced in Fig. 6.

In the next few figures graphs of characteristic examples are shown for the other observed parameters. In Fig. 7 an internal bending moment M_z is introduced for the case of variation of the parameter k_2 . The

influence of the variation is the most significant for the values of parameter around the nominal value. Therefore also this parameter must not be excluded.

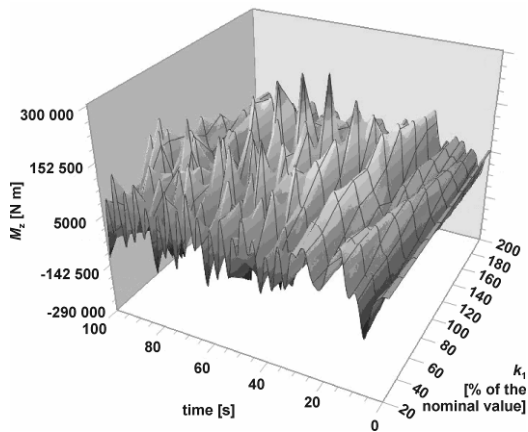


Figure 6. The bending moment M_z , when the influence of the parameter k_1 is observed

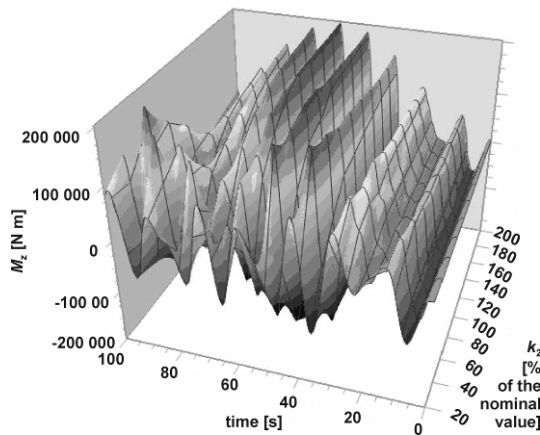


Figure 7. The bending moment M_z , when the influence of the parameter k_2 is observed

In Fig. 8 an internal bending moment M_z is introduced for the case of variation of the parameter k_z . The influence of the variation is noticeable for the values of parameter lower than nominal value. For the nominal value of the stiffness k_z and higher values the influence of the variation is insignificant.

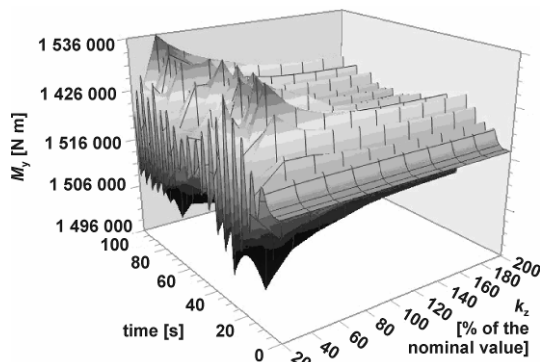


Figure 8. The bending moment M_z , when the influence of the parameter k_L is observed

The same insignificant influence of the variation is noticeable on the graphs (not shown) of other output

quantities as are α_R , α_T , M_y and M_t . For this reason the assumption of non-deformability of the crane's tower in z -direction is appropriate.

Similar graphs can be shown for the parameters k_x and k_L and the same conclusion can be made about the non-deformability of the jib in x -direction and of the load carrying rope along its length.

The influences of the damping coefficients and coefficients of the air resistance (d_1 , d_2 , d_x , d_z , d_1 , $d_{ar 2}$ and $d_{ar 3}$) are also negligible. The sample graph is shown in Fig. 9.

The introduced graphs clearly show the influence of changes of the individual parameters on the dynamic response of the crane's structure. Therefore these graphs can be used as a tool for the selection of the parameters which have enough insignificant influence that they can be neglected.

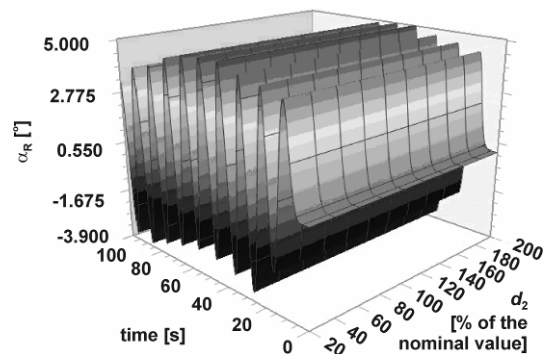


Figure 9. The load swinging angle in the radial direction α_r , when the influence of the parameter d_2 is observed

On the basis of this selection the following degrees of freedom are chosen to be excluded from the enhanced model: extension of the tower in z direction (parameters k_z and d_z), extension of the jib in x direction (parameters k_x and d_x) and extension of the load carrying rope (parameters k_L and d_L).

With this action the number of degrees of freedom and related number of the equations of the enhanced mathematical model is preserved on the fairly low level ($11-3=8$) and the acceptable processing times is ensured without losing the accuracy.

3. THE RESULTS

In this chapter the results of simulations with the basic and with the enhanced mathematical model are shown in the single graphs together with the measured results enabling direct comparison. The main aim of the comparison in this case is to confirm the hypothesis that the enhanced mathematical model (Fig. 3) is more accurate than the basic model (Fig. 1). Therefore, both mathematical models were used for the simulations and the physical model was used for the measurements. To allow a comparison between these three models, the input data from the physical model were used for the simulations.

The following part of the crane's working-cycle was observed: the acceleration of the rotation of the jib from

zero to the maximum angular velocity in time t_1 ; the rotation of the platform with constant angular velocity in time t_2 ; the deceleration of the platform's rotation from the maximum angular velocity to zero in time t_3 ; the observation of the crane after the stopping of the rotation in time t_4 . A payload was suspended from the jib during the entire cycle.

The simulations and the measurements were carried out with a range of load masses ($m_Q = 20$ to 50 kg), different radii of the suspension point ($R_0 = 1$ to 2 m), and different lengths of the load-carrying rope ($L_0 = 0.5$ to 2 m). The effects of the various types of acceleration and deceleration on the trajectory of the suspended load were also studied, including the changes to the acceleration time and the average acceleration. The results for four examples, defined by tables 1 and 2, are shown in the figures below. From the chosen length of the load-carrying rope $L_0 = 2$ m, the period of oscillation of the suspended payload, looked at as a mathematical pendulum, can be calculated as $t_Q = 2.84$ s.

Table 1. Selected values of the acceleration time t_1

	Example 1	Example 2	Example 3	Example 4
t_1 [s]	$t_Q / 4 = 0.71$	$t_Q / 2 = 1.42$	$t_Q = 2.84$	$3t_Q / 2 = 4.26$

Table 2. Values of the other parameters

Parameter	Value
t_2	8 s
t_3	$= t_1$
$t_1 + t_2 + t_3 + t_4$	14 s (18 s)
$\dot{\varphi}_{0,\max}$	0.738 rad/s
m_Q	50 kg
R_0	2 m
$L_0 L_0$	2 m
acceleration/deceleration type	constant value

From Figs. 10 and 11 the pendulum motion of the suspended payload for Example 1 can be seen. Figures 12 to 14 introduce the crane's dynamic loading. In these figures, and in Figs. 15 to 20, the thin, continuous line represents the graph of measured values, whereas the bold continuous line represents the simulated data, created with the enhanced mathematical model. The data created with the basic mathematical model are marked with an asterisk and represented on the graph with a dashed line. The graph representing the angle φ_0 of rotation of the driving shaft is also shown, introducing the phases of the input angular velocity $\dot{\varphi}_0(t)$.

In Fig. 11 the tangential angle α_T of the load sway is introduced. This angle can be compared with the in-plane load sway under the conditions of the translation of the payload's suspension point. In the acceleration phase a degree of payload lag can be observed. The

maximum lag is observed immediately after this phase. The simulated value of the lag is 25.4% greater than the measured one. This is an improvement in comparison with the previous model, where the deviation was minus 6.5%.

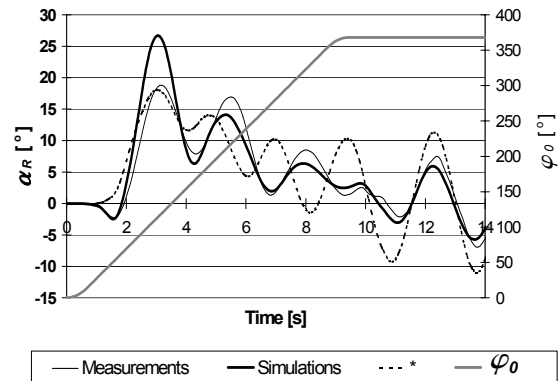


Figure 10. Radial (α_R) angle of the load sway with respect to time for Example 1

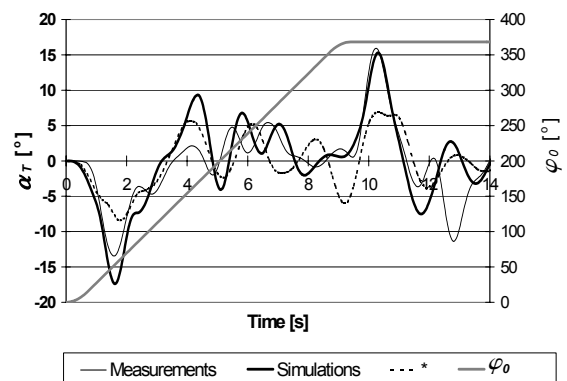


Figure 11. Tangential (α_T) angle of the load sway with respect to time for Example 1

The quantitative improvement is upgraded because the actual simulated value is greater than the measured one, so representing a conservative solution. The phase of moving with a constant speed is denoted by oscillations, the mean value of which is close to the static equilibrium. In the deceleration phase the payload is forestalling the suspension point, and finally, after the rotation stops, damped oscillations develop around the static equilibrium. The maximum positive peak value is encountered right after the rotation stops. The simulated value of this peak is nearly the same as the measured one (-3.0%). In the case of the basic model, the deviation is much bigger.

In Fig. 10 the radial angle α_R of the load sway is introduced; this angle is initially a consequence of the centrifugal force, which is caused by the rotation of the crane. The radial angle α_R is therefore unique to slewing cranes. The oscillation of its value with respect to time is a consequence of the fact that this angle is coupled with the tangential angle, and is therefore influenced by it. In addition, the radial angle also has an influence on the tangential angle. In the first moment of the acceleration phase, an apparent shift of the payload in the radial direction is encountered (a negative value of α_R). This is the result of the rotation of the local coordinate system $\xi\eta\zeta$ and of the movement of its

origin, which is located at the payload's suspension point. This effect is noticeable in the measured and in the enhanced simulated cases. The difference in the peak values is 7.5%. In the case of the basic simulation the apparent shift was not detected. The positive peak value of the radial angle (α_R) is achieved in the phase of rotation with constant speed. The comparison shows that the simulated peak value is about 40% higher than the measured one. The quantitative difference is, in this case, greater than it is in the case of the basic mathematical model. On the other hand, the simulated value is now greater than the measured one, so representing a conservative solution. In addition, the overall qualitative and quantitative agreement is much better in the case of the enhanced model. The comparison shows that there is no phase shift between the simulated and measured curves. In addition, the maximum negative peak value, which occurs after the deceleration, differs by 16.8% in comparison with the measured one, whereas the difference in the case of the basic mathematical model is 57.7%.

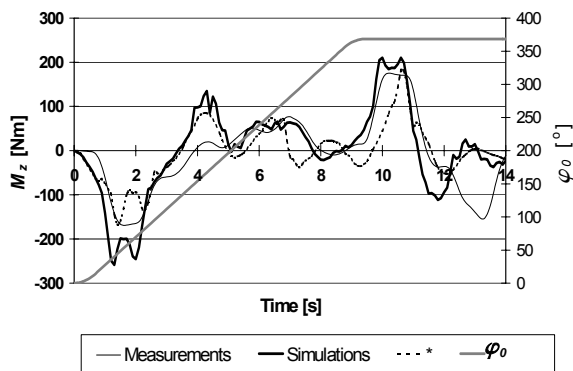


Figure 12. Bending moment in the jib around the z-axis (M_z) for Example 1

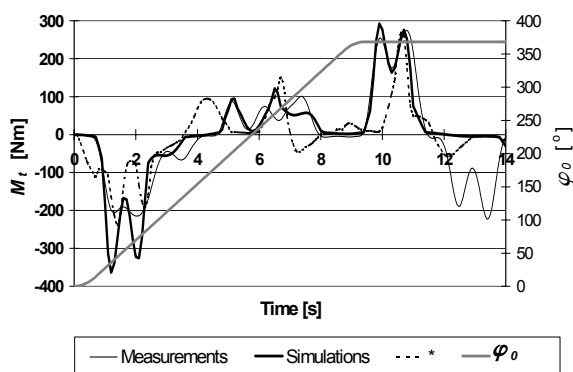


Figure 13. Torsion moment in the driving shaft (M_t) for Example 1

The bending moment in the jib around the z-axis is shown in Fig. 12, and the torsion moment in the driving shaft is shown in Fig. 13. The graphs for both moments are similar because they are both caused by horizontal inertial forces acting in a tangential direction. An improved qualitative agreement between the curves is observed in the case of the enhanced mathematical model. The quantitative agreement is not as good. The difference in the maximum negative peak value is bigger than in the case of the basic model; however, in

the case of the maximum positive peak value this difference is almost unchanged. The results in the case of the enhanced mathematical model show higher values of the moment than is the case with the measurements and are therefore of a conservative nature.

The bending moment in the jib around the y-axis is shown in Fig. 14. Its mean value is defined by the weight of the payload and the weight of specific parts of the crane. The oscillation of its value with respect to time is a consequence of the dynamic effects of the payload's spatial sway in the foreground. A very much improved qualitative agreement between the curves is clear in the case of the enhanced mathematical model. In addition, the quantitative agreement is also improved. The maximum difference in the peak values, which appear right after the acceleration phase, is 8.5%, whereas the difference in the peak values after the deceleration phase is almost zero. The conservative nature of the results is also clear.

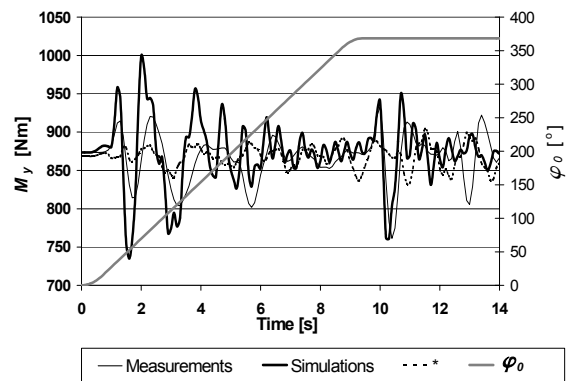


Figure 14. Bending moment in the jib around the y-axis (M_y) for Example 1

In the following figures the results for Examples 2 to 4 are shown. Because they are more interesting, only the graphs of the bending moments are presented. For all the graphs, very similar remarks to those used for Example 1 could be written. A significant improvement in the qualitative agreement of the results is supplemented by a quantitative improvement and the conservative nature of the simulated results. In the case of the bending moment in the jib around the y-axis (M_y), another improvement is noticeable (Fig. 16): the definition of the moment's static value is enhanced and the error in its initial value is eliminated.

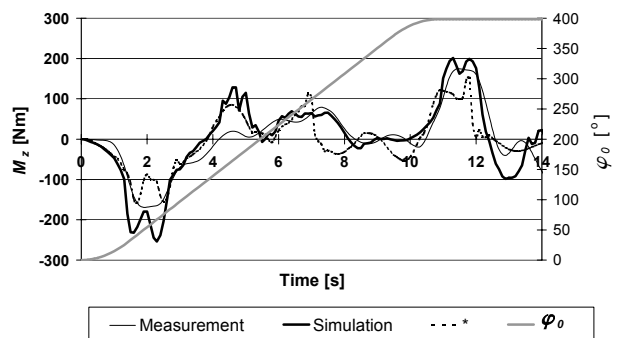


Figure 15. Bending moment in the jib around the z-axis (M_z) for Example 2

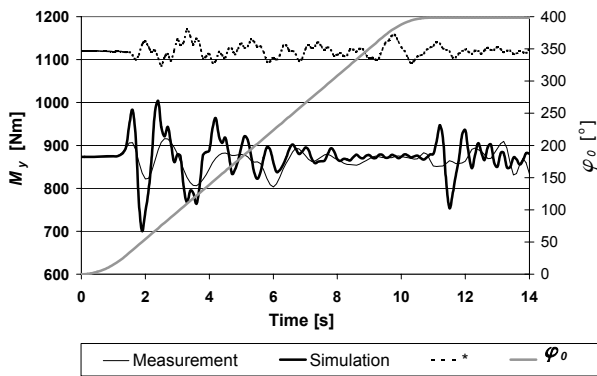


Figure 16. Bending moment in the jib around the y -axis (M_y) for Example 2

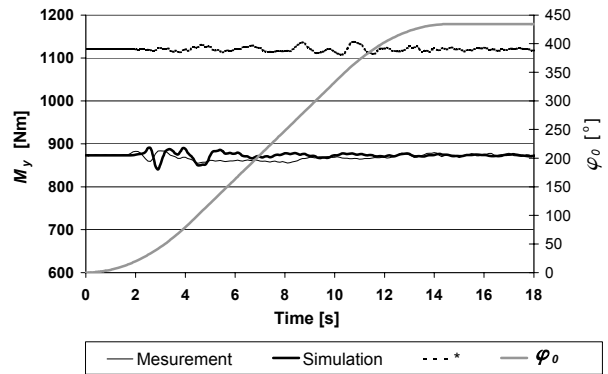


Figure 20. Bending moment in the jib around the y -axis (M_y) for Example 4

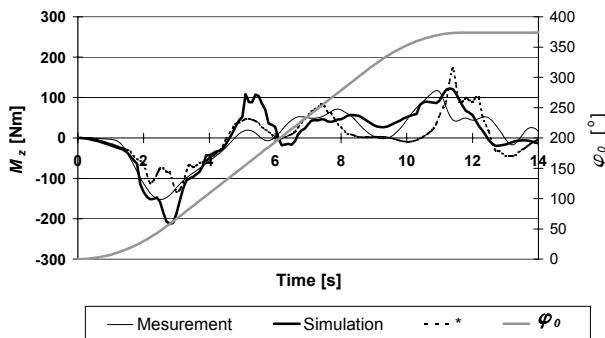


Figure 17. Bending moment in the jib around the z -axis (M_z) for Example 3

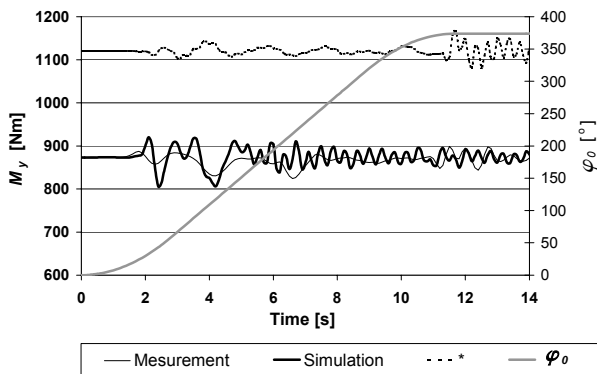


Figure 18. Bending moment in the jib around the y -axis (M_y) for Example 3

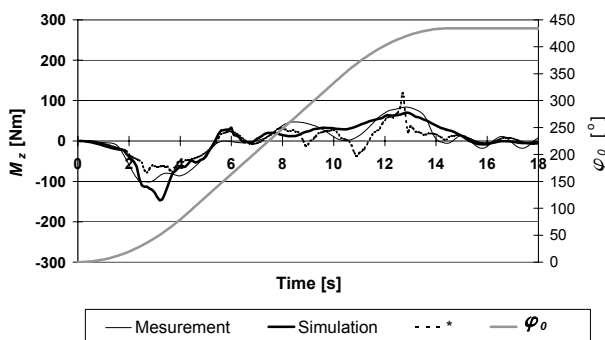


Figure 19. Bending moment in the jib around the z -axis (M_z) for Example 4

4. CONCLUSION

Basic and enhanced mathematical models of a slewing crane are briefly presented. The enhanced model is developed on the basis of experiences with a basic model. Two additional mass elements enable a more realistic mathematical description of this real-world problem. An increase in the number of degrees of freedom of the model was prevented by neglecting several of the less significant influences. Lagrange equations were used to derive the equations of motion, and a computer program was developed to solve these equations.

For the purpose of evaluation, measurements were made on the physical model. A detailed comparison was carried out between the measured results and the results of the simulations with the basic model and the enhanced mathematical model.

A large overall improvement in the qualitative and quantitative matching of the results for the case of the enhanced mathematical model was established. The improvement in the accuracy of the results is noticeable, especially during the deceleration phase of the crane's rotation, where in the case of the basic model larger differences were encountered. Now, the simulated results are also conservative in nature, because the simulated loads are very close to or bigger than the measured results. The biggest improvement is encountered in the case of the bending moment in the jib around the y -axis (M_y), where its dynamic behaviour is much more realistic and the shift in its initial value is eliminated.

As was the case with the basic mathematical model, also the newly derived model has no restrictions in terms of small angles of the load sway. This makes it possible to study of the crane's behaviour under extreme conditions, as is the case in the examples shown, where the values of the radial angle (α_R) go up to 27° .

By deriving the enhanced non-linear mathematical model and confirming its superiority in comparison with the basic one, the importance of selecting the appropriate model is shown. For an additional improvement of the results, efforts should be directed to redefine the elastic and damping properties of the

structure. The non-linear characteristics of the elements connecting the driving motor with the rotating platform should be in the first plane.

ACKNOWLEDGMENT

The author would like to thank assoc. prof. Dr. Janez Kramar from the Faculty of Mechanical Engineering, Ljubljana, Slovenia, for all his support, and without whom this research would not have been possible.

REFERENCES

- [1] Onishi, E., Tsuboi, I., Egusa, T., Uesugi, M.: Automatic control of an overhead crane, Proceedings of the Eight Triennial IFAC World Congress, Volume 4: A. Mechanical Systems and Robots, pp.1885-1890, Pergamon Press, 1982.
- [2] Lee, H.: A new design approach for the anti-swing trajectory control of overhead cranes with high-speed hoisting. International Journal of Control, 77(10), pp. 931-940, 2004.
- [3] Yavin, Y., Kemp, P.D.: The application of extended inverse dynamics control, Computers and Mathematics with Applications, 40, pp. 669-677, 2000.
- [4] Cheng, C.C., Chen, C.Y.: Controller design for an overhead crane system with uncertainty. Control Eng Practice, 4(5), pp. 645-653, 1996.
- [5] Moustafa, K.A.F.: Feedback control of overhead cranes swing with variable rope length, Proceedings of the American Control Conference, Part 1, pp. 691-695, Baltimore, MD, USA, Jun 29-Jul 1, 1994.
- [6] Spathopoulos, M.P., Fragopoulos, D.: Pendulation control of an offshore crane, International Journal of Control, 77(7), pp. 654-670, 2004.
- [7] Glossiotis, G., Antoniadis, I.: Payload sway suppression in rotary cranes by digital filtering of the commanded inputs, Proceedings of the Institution of Mechanical Engineers, Part K, Journal of Multi-body Dynamics, 217(2), pp. 99-109, 2003.
- [8] Posiadała, B., Skalmierski, B., Tomski, L.: Motion of the lifting load broth by a kinematic forcing of the crane telescopic boom, Mechanisms and Machine theory, 25(5), pp. 547-556, 1990.
- [9] Jerman, B., Podržaj, P., Kramar, J.: An Investigation of Slewing-Crane Dynamics During Slewing Motion - Development and Verification of a Mathematical Model, International Journal of Mechanical Sciences, 46(5), pp. 729-750, 2004.
- [10] Abdel-Rahman, E.M., Nayfeh, A.H., Masoud, Z.N.: Dynamics and Control of Cranes: A Review. Journal of Vibration and Control, 9, pp. 863-908, 2003.
- [11] Lee, J.-W., Kim, D.-H.: Dynamics of a spreader suspended by four flexible cables, Proceedings of the Institution of Mechanical Engineers, Part C, Journal of Mechanical Engineering Science, 218(10), pp. 1125-1138, 2004.
- [12] Lee, J.-W., Kim, D.-H., Oh, J.-H.: A unified approach to the kinematics of a spreader suspended by multiple cables, Proceedings of the Institution of Mechanical Engineers, Part C, Journal of Mechanical Engineering Science, 217(3), pp. 289-312, 2003.
- [13] Huilgol, R.R., Christie, J.R., Panizza, M.P.: The motion of a mass hanging from an overhead crane, Chaos, Solitons and Fractals, 5(9), pp. 1619-1631, 1995.
- [14] Moustafa, K.A.F., Ebeid, A.M.: Nonlinear modeling and control of overhead crane load sway, J. Dyn. Syst. Meas. Control Trans ASME, 110, pp. 266-271, 1988.
- [15] Oguamanam, D.C.D., Hansen, J.S.: Dynamics of a three-dimensional overhead crane system, Journal of Sound and Vibration, 242(3), pp. 411-426, 2001.
- [16] Wu, J.J., Whittaker A.R., Cartmell, M.P.: The use of finite element techniques for calculating the dynamic response of structures to moving loads, Computers and Structures, 78, pp. 789-799, 2000.
- [17] Vähä, P., Voutilainen, D.O.: Dynamics of a closed kinematic Chain Crane with a suspended Load. Sähkö - Electricity and electronics, 61(6), pp. 42-61, 1988.
- [18] Ghigliazza, R.M., Holmes, P.: On the dynamics of cranes, or spherical pendula with moving supports. Int. J. of Non-Linear Mechanics, 37, pp. 1211-1221, 2002.
- [19] Lau, W.S.M., Low, K.H.: Motion Analysis of suspended Mass attached to a Crane. Computers and Structures, 52(1), pp. 169-178, 1994.
- [20] Wei, L., Zhixin, W., Baoliang, Q., Shijun, S., Caishan, L.: The Mathematical Model of the Load vibration-sway on fixed Type Tower Cranes. Modeling, Measurement & Control B: Solid & Fluid Mechanics & Thermics, Mechanical Systems, Robotics, Civil engineering, 51(3), pp. 1-12, 1993.
- [21] Matthias, K., Kirsten, N.: Dynamische beanspruchung im dreh - und wippwek von doppelnenker - wippdrehkranen - Teil 1. Hebezeuge und Fördermittel, 9, pp. 278-279, 1984.
- [22] Matthias, K., Kirsten, N.: Dynamische beanspruchung im dreh - und wippwek von doppelnenker - wippdrehkranen - Teil 2. Hebezeuge und Fördermittel, 10, pp. 303-305, 1984.
- [23] Schaufuss, J.: Beanspruchungs-zeit-funktionen für krandrehwerke, Hebezeuge und Fördermittel, 8, pp. 242-245, 1983.
- [24] Cartmell, M. P., Morrish, L., Taylor, A.J.: Dynamics of Spreader Motion in a Gantry Crane, Proceedings of the Institution of Mechanical Engineers, Part C, Journal of Mechanical Engineering Science, 212(2), pp. 85-105, 1998.
- [25] Lazan, B.J.: *Damping of materials and members in structural mechanics*, First Edition, Pergamon Press, 1968.